

**Electron and nuclear spin polarization in Rb-Xe spin-exchange optical hyperpolarization**Matti Hanni,<sup>1,2,\*</sup> Perttu Lantto,<sup>2</sup> Michal Repiský,<sup>3</sup> Jiří Mareš,<sup>2</sup> Brian Saam,<sup>4</sup> and Juha Vaara<sup>2,\*</sup><sup>1</sup>*Medical Research Center, University of Oulu and Oulu University Hospital, P.O. Box 8000, FI-90014 Oulu, Finland;**Department of Diagnostic Radiology, Oulu University Hospital, P.O. Box 50, FI-90029 Oulu, Finland;**and Research Unit for Medical Imaging, Physics and Technology, University of Oulu, P.O. Box 8000, FI-90014 Oulu, Finland*<sup>2</sup>*NMR Research Unit, University of Oulu, P.O. Box 3000, FI-90014 Oulu, Finland*<sup>3</sup>*CTCC, Department of Chemistry, University of Tromsø, NO-9037 Tromsø, Norway*<sup>4</sup>*Department of Physics and Astronomy, University of Utah, Salt Lake City, Utah 84112, USA*

(Received 9 August 2016; published 31 March 2017)

Spin-exchange optical hyperpolarization of  $^{129}\text{Xe}$  gas enhances the signal-to-noise ratio in nuclear magnetic resonance experiments. The governing parameter of the Rb-Xe spin-exchange process, the so-called enhancement factor, was recently reevaluated experimentally. However, the underlying hyperfine coupling and atomic interaction potential as functions of the internuclear distance of the open-shell Rb-Xe dimer have not been accurately determined to date. We present a piecewise approximation based on first-principles calculations of these parameters contributing to the NMR and EPR frequency shifts in the low-density Rb-Xe gas mixture of relevance to hyperpolarization experiments. Both Rb electron and  $^{129}\text{Xe}$  nuclear spin polarizations are estimated based on a combination of electronic-structure calculations, observed frequency shifts, and an estimate of the Rb number density. Finally, an expression for the enhancement factor in terms of modern electronic-structure theory is obtained.

DOI: [10.1103/PhysRevA.95.032509](https://doi.org/10.1103/PhysRevA.95.032509)**I. INTRODUCTION**

The use of hyperpolarized noble gases, such as  $^{129}\text{Xe}$ ,  $^{83}\text{Kr}$ , and  $^3\text{He}$ , significantly helps to overcome the central problem of weak signal in noble-gas nuclear magnetic resonance (NMR) spectroscopy [1,2] and magnetic resonance imaging [3,4] experiments. Hyperpolarization also plays a vital role in atomic magnetometry [5],  $^{129}\text{Xe}$  NMR biosensors [6], and many other specialized applications, such as *in vivo*  $^{129}\text{Xe}$  NMR detection of cells [7], as well as the optical detection of  $^{129}\text{Xe}$  NMR in a microfluidic chip [8]. Spin-exchange optical pumping (SEOP) is an important hyperpolarization (HP) technique [9], in which the unpaired electrons of rubidium atoms are laser polarized, and subsequently, the achieved polarization is transferred to the nuclei of noble-gas atoms in a gas mixture containing the two species, as well as buffer gases such as He and  $\text{N}_2$ . The polarization exchange occurs due to the magnetic hyperfine interactions between the electron spin of the alkali metal and noble-gas nuclear spin. These interactions can be represented by the so-called enhancement factor  $\kappa$  [10,11] that is directly related to the observed frequency shifts in both the NMR and electron paramagnetic resonance (EPR) regimes. However, the enhancement factor can also be evaluated microscopically using first-principles quantum-mechanical electronic-structure calculations. As shown in this article, the empirical enhancement factor is proportional to the  $^{129}\text{Xe}$  hyperfine coupling constant (HFCC) resulting from the interactions with Rb atoms and corresponding to the leading nontrivial term in the appropriate virial expansion [12]. For the calculation of the temperature-dependent quantum-mechanical equivalent of the enhancement factor, the second virial coefficient of the  $^{129}\text{Xe}$  HFCC, one needs detailed knowledge of the internuclear distance dependence of both the hyperfine coupling constant

and the interatomic potential-energy function in the open-shell Rb-Xe dimer.

The  $^{129}\text{Xe}$  NMR and EPR frequency shifts occurring in SEOP experiments have been observed for years [10,11,13]. A major advance in the detection of the  $^{129}\text{Xe}$  NMR frequency shift in the Rb-Xe gas mixture has recently taken place, leading to a reevaluation of the value of the enhancement factor [11]. Despite the growing knowledge and number of experimental applications of HP techniques, only a handful of first-principles modeling studies have been performed in the field of HP physics [14–16], mainly discussing the role of the anisotropic HFCC as a limiting relaxation factor in HP experiments [9]. To date, no detailed first-principles theoretical understanding of the NMR and EPR frequency shifts occurring in the SEOP process in dilute Rb-Xe gas mixtures has been pursued, beyond early approaches employing semiempirical calculations [10,17]. Here, we use state-of-the-art electronic-structure calculations to provide theoretical estimates of the  $^{129}\text{Xe}$  HFCC in the Rb-Xe dimer as a function of the internuclear separation. This parameter, averaged over the corresponding Rb-Xe potential-energy curve (PEC), is the essential factor contributing to the NMR and EPR frequency shifts [11] in the gaseous conditions characteristic of SEOP experiments. We report a highly electron correlated Rb-Xe PEC using the relativistic pseudopotential technique, which can be used, in addition to SEOP studies, in the theoretical description of the bonding characteristics in weakly bound van der Waals molecules [18,19]. The investigation of the present Rb-Xe PEC draws heavily from our earlier work on Xe-Xe PEC [20]. A combination of various electronic-structure methods is used to provide a relativistic, electron-correlated approximation of the  $^{129}\text{Xe}$  HFCC, involving all-electron spin polarization. We show that by using a combination of first-principles computational methodology and the measured NMR and EPR frequency shifts, it is possible to predict the experimentally little known physical parameters in SEOP experiments, the Rb

\*Corresponding authors: matti.hanni@oulu.fi, juha.vaara@iki.fi

electron spin polarization,  $P_S = 2\langle S_z \rangle$  (with the Rb number density evaluated based on the relation of Killian [21]; see below), and, most importantly, the degree of  $^{129}\text{Xe}$  nuclear spin polarization  $P_{\text{Xe}}$ . These belong to the most crucial physical parameters in the current and future development of SEOP-based magnetic resonance techniques [1–3,8,22].

## II. EPR AND NMR FREQUENCY SHIFTS

Starting from the Breit-Rabi formula for the hyperfine energy levels of a system with an unpaired electron and a spin- $\frac{1}{2}$  nucleus in a magnetic field [23], one can derive the equation for the change of the EPR frequency of the  $^{87}\text{Rb}$  atom due to the interaction with noble-gas atoms. The  $^{129}\text{Xe}$  HFCC can be used to parametrize both the NMR and EPR frequency shifts. In a low-density Rb-Xe gas mixture, the leading-order change of the HFCC can be written using the second virial coefficient  $A_{\text{Xe},1}^{\text{iso}}$  [12] of the  $^{129}\text{Xe}$  HFCC, which incorporates only the pair interactions between the Rb and Xe species. Detailed derivations of the aforementioned parameters are included in the following.

### A. EPR shift

The EPR frequency, for the special case of a  $^{87}\text{Rb}$  atom with one unpaired electron in the presence of Xe atoms, can be written in the form of the well-known Breit-Rabi equation [23]:

$$\nu_{m_F} = E_{m_F}/h = -\frac{\nu_{\text{HF}}}{2(2I+1)} \pm \left[ 1 + \frac{2m_F}{I+\frac{1}{2}} \left( \frac{g\mu_B}{h\nu_{\text{HF}}} B \right) + \left( \frac{g\mu_B}{h\nu_{\text{HF}}} B \right)^2 \right]^{\frac{1}{2}}. \quad (1)$$

Here,  $I = \frac{3}{2}$  is the  $^{87}\text{Rb}$  nuclear spin quantum number,  $\nu_{\text{HF}} = 2A_{\text{Rb}}^{\text{iso}}$  is the hyperfine splitting in the absence of magnetic fields,  $A_{\text{Rb}}^{\text{iso}}$  is the  $^{87}\text{Rb}$  HFCC,  $g$  is the electron  $g$  factor,  $\mu_B$  is the Bohr magneton,  $h$  is Planck's constant, and  $B$  is the total magnetic flux density, arising both from the external field and from the nuclear spin polarization of the Xe atoms present in the gas. Equation (1) yields the energy for the hyperfine transition between two substates,  $|F, m_F\rangle$  and  $|F, m_F - 1\rangle$ , of the total spin angular momentum  $F$ . In the  $F = I + S = I + \frac{1}{2}$  manifold, corresponding to the plus sign in Eq. (1) [24], the transition frequency can be written as

$$\begin{aligned} \nu_{m_F} - \nu_{m_F-1} &= \frac{E_{m_F}}{h} - \frac{E_{m_F-1}}{h} \\ &= \frac{\nu_{\text{HF}}}{2} \left[ \sqrt{1 + \frac{2m_F}{I+\frac{1}{2}} x + x^2} - \sqrt{1 + \frac{2(m_F-1)}{I+\frac{1}{2}} x + x^2} \right], \end{aligned} \quad (2)$$

where  $x = \frac{g\mu_B}{h\nu_{\text{HF}}} B$ . For small  $x$ , the square root can be expanded to yield

$$\sqrt{1 + ax + x^2} \approx 1 + \frac{a}{2}x + \frac{1}{4}\left(2 - \frac{a^2}{2}\right)x^2, \quad (3)$$

and Eq. (2) can be approximated as

$$\nu_{m_F} - \nu_{m_F-1} \approx \frac{\nu_{\text{HF}}}{2I+1} \left[ x - \frac{2}{2I+1} \left( m_F - \frac{1}{2} \right) x^2 \right]. \quad (4)$$

This transition frequency depends on both  $B$  and (via  $\nu_{\text{HF}}$ )  $A_{\text{Rb}}^{\text{iso}}$ , so its total differential in terms of these quantities can be used to evaluate the interaction effect on the EPR transition frequency. In particular, we write

$$\begin{aligned} d(\nu_{m_F} - \nu_{m_F-1}) &= \frac{\partial(\nu_{m_F} - \nu_{m_F-1})}{\partial B} dB \\ &\quad + \frac{\partial(\nu_{m_F} - \nu_{m_F-1})}{\partial A_{\text{Rb}}^{\text{iso}}} dA_{\text{Rb}}^{\text{iso}}. \end{aligned} \quad (5)$$

The derivatives in the first and second terms of this equation can, using the chain rule, be written as

$$\begin{aligned} \frac{\partial(\nu_{m_F} - \nu_{m_F-1})}{\partial B} &= \frac{\partial(\nu_{m_F} - \nu_{m_F-1})}{\partial x} \frac{\partial x}{\partial B} \\ &= \frac{g\mu_B}{h(2I+1)} \left[ 1 - \left( m_F - \frac{1}{2} \right) \frac{4}{2I+1} x_0 \right], \quad (6) \\ \frac{\partial(\nu_{m_F} - \nu_{m_F-1})}{\partial A_{\text{Rb}}^{\text{iso}}} &= \frac{\partial(\nu_{m_F} - \nu_{m_F-1})}{\partial \nu_{\text{HF}}} \frac{\partial \nu_{\text{HF}}}{\partial A_{\text{Rb}}^{\text{iso}}} \\ &= \frac{4}{(2I+1)^2} \left( m_F - \frac{1}{2} \right) x_0^2, \quad (7) \end{aligned}$$

where  $x_0 = \frac{g\mu_B}{h\nu_{\text{HF}}} B_0$  corresponds to the static external field  $B_0$ . Now, Eq. (5) becomes

$$\begin{aligned} d(\nu_{m_F} - \nu_{m_F-1}) &= \frac{g\mu_B}{h(2I+1)} \\ &\quad \times \left[ 1 - \left( m_F - \frac{1}{2} \right) \frac{4}{2I+1} x_0 \right] dB \\ &\quad + \frac{4}{(2I+1)^2} \left( m_F - \frac{1}{2} \right) x_0^2 dA_{\text{Rb}}^{\text{iso}}. \end{aligned} \quad (8)$$

Consequently, altogether, three terms are responsible for the  $^{87}\text{Rb}$  frequency shift. The first two terms depend on  $dB$ , the additional magnetic flux density due to the Xe nuclear magnetization in the sample. The third term arises from the changes caused by the Xe atoms to the  $^{87}\text{Rb}$  HFCC in the Rb-Xe gas mixture. This term can be evaluated by writing

$$dA_{\text{Rb}}^{\text{iso}} = A_{\text{Rb},1}^{\text{iso}}[\text{Xe}], \quad (9)$$

where  $A_{\text{Rb},1}^{\text{iso}}$  and  $[\text{Xe}]$  are the second virial coefficient of the  $^{87}\text{Rb}$  hyperfine coupling in the Rb-Xe dimer and the xenon number density, respectively. We neglect the three-body and higher-order contributions to the appropriate virial expansion, which is a valid approximation for the dilute gas admixture considered here (see Sec. II E). Numerical calculations at an accessible magnetic field of 2.7 mT at temperatures valid for experiments (140 °C–220 °C) produce a frequency shift of roughly  $-5$  Hz from the third term in Eq. (8), using our presently calculated (see Sec. III A) value of  $A_{\text{Rb},1}^{\text{iso}} \approx -15400 \text{ MHz } \text{\AA}^3$  at 2.7 mT in the Rb-Xe dimer, as well as a realistic value of 0.074 amagat for the xenon number density  $[\text{Xe}]$  [25]. This shift contribution amounts to only about 0.1% of the magnitude of the leading term,  $\frac{g\mu_B}{h(2I+1)} dB$ , evaluated

using Eqs. (18) and (19) below. This figure was arrived at by using the experimentally feasible Xe nuclear spin polarization  $P_{Xe} = 0.32$  in the same number density and temperature range as above but now with our calculated value for the second virial coefficient of the Xe hyperfine coupling  $A_{Xe,1}^{iso}$ . The corresponding interaction-induced changes of  $A_{Xe}^{iso}$  due to the other gas species present in SEOP experiments, He and  $N_2$ , might also play a role [11,26]. However, as no hyperfine interactions take place between these species and xenon, their effect is inevitably smaller than the effect of rubidium. This is computationally verified by the close correspondence of our present and most recent experimental [25]  $\kappa$  values (see Table II below).

Among the two terms proportional to  $dB$ , only the leading term is important since  $(m_F - \frac{1}{2}) \frac{4}{2I+1} x_0$  equals 0.017 at an applied field of 2.7 mT, with  $m_F = 2$  and  $\nu_{HF} = 6384.682610$  MHz [27], which amounts to only about 2% of the magnitude of the leading term. Hence, we conclude that the most important term in the EPR frequency shift is the leading term emerging from the change in the magnetic field  $dB$ .

### B. Empirical formula for the EPR shift

We can derive the EPR frequency shift caused by the presence of the spin-polarized Xe gas in two different ways. The first derivation yields an empirical formula for the quantity. Besides the external magnetic field, an additional field arising from a spherical, uniformly magnetized sample of Xe atoms can be written as

$$B = \frac{2\mu_0}{3} M_{Xe}, \quad (10)$$

where the magnetization equals

$$M_{Xe} = [Xe] \gamma_{Xe} \hbar \langle I_{Xe} \rangle. \quad (11)$$

In Eq. (11), the polarization  $P_{Xe}$  is defined by  $\langle I_{Xe} \rangle = P_{Xe} I_{Xe}$ , where  $I_{Xe} = \frac{1}{2}$  is the nuclear spin; the  $^{129}\text{Xe}$  gyromagnetic ratio is given by  $\gamma_{Xe} = \frac{\mu_{Xe}}{\hbar I_{Xe}}$ , where  $\mu_{Xe}$  is the  $^{129}\text{Xe}$  nuclear magnetic moment. The electron cloud of the Rb atom strengthens the magnetic field at the site of the  $^{87}\text{Rb}$  nucleus by the factor  $\kappa$ , thus allowing us to write  $dB$  as

$$dB = \kappa \frac{2\mu_0}{3} M_{Xe} = \kappa \frac{2}{3} \mu_0 [Xe] \mu_{Xe} P_{Xe}. \quad (12)$$

By multiplying Eq. (12) with the leading coefficient in Eq. (8), we arrive at an empirical formula for the EPR frequency shift [10,11]:

$$\Delta\nu_{Rb} = \frac{g\mu_B}{h(2I+1)} \kappa \frac{2}{3} \mu_0 [Xe] \mu_{Xe} P_{Xe}. \quad (13)$$

### C. Microscopic equivalent of the enhancement factor

The second formulation for the EPR shift stems from a quantum-chemical description of the EPR spin Hamiltonian. The Zeeman interaction of the unpaired electron can be written as

$$H_Z = \mu_B \vec{B} \cdot \vec{g} \cdot \vec{S}, \quad (14)$$

where  $\vec{g}$  is the  $g$  tensor,  $\vec{B}$  is the magnetic field, and  $\vec{S}$  is the electron spin operator. As noted above, part of the field

arises from the spin-polarized Xe nuclei. This contribution can be parameterized by the hyperfine coupling term of the spin Hamiltonian,

$$H_{hf} = \vec{S} \cdot \vec{\bar{A}}_{Xe} \cdot \vec{I}_{Xe}, \quad (15)$$

where  $\vec{\bar{A}}_{Xe}$  arises from the dipolar and contact fields on the unpaired electron from the interaction with a single Xe nucleus in the environment ( $\vec{I}_{Xe}$  is the nuclear spin operator). An expression for the effective, additional field  $dB$  is obtained by equating  $H_Z = H_{hf}$ . For the case of an isotropic gas phase, we can write Eq. (14) in terms of the isotropic rotational averages of the  $g$  and  $\vec{\bar{A}}_{Xe}$  tensors (the  $g$  factor and the HFCC  $A_{Xe}^{iso}$ , respectively) as

$$\mu_B S_z g dB = S_z A_{Xe}^{iso} \langle I_{Xe} \rangle = S_z A_{Xe}^{iso} P_{Xe} I_{Xe}. \quad (16)$$

This yields, for the average field caused by a single Xe atom,

$$dB = A_{Xe}^{iso} \frac{P_{Xe} I_{Xe}}{g\mu_B}. \quad (17)$$

Here, we can again employ the leading term of the virial expansion to collect the effect of all the Rb-Xe pairs in the gas to the field  $dB$ :

$$dB \approx B_{Rb,1}[Xe] = A_{Xe,1}^{iso} \frac{P_{Xe} I_{Xe}}{g\mu_B} [Xe], \quad (18)$$

where  $B_{Rb,1}$  and  $A_{Xe,1}^{iso}$  are the second virial coefficients of the magnetic flux density at the Rb atom and  $^{129}\text{Xe}$  HFCC, respectively. With the prefactor from Eq. (8), we obtain a second formulation for the EPR frequency shift, which is based on well-defined microscopic quantities that lend themselves straightforwardly to first-principles computation:

$$\Delta\nu_{Rb} = \frac{1}{h(2I+1)} A_{Xe,1}^{iso} P_{Xe} I_{Xe} [Xe]. \quad (19)$$

We can now equate the two expressions for the EPR frequency shifts [Eqs. (13) and (19)] and arrive at a formula for the empirical enhancement factor in terms of  $A_{Xe,1}^{iso}$ ,

$$\kappa = \frac{3}{2} A_{Xe,1}^{iso} \frac{1}{g\mu_B \mu_0 \gamma_{Xe} \hbar}. \quad (20)$$

Since the second virial coefficient of the hyperfine coupling depends on the temperature (see below), Eq. (20) suggests a way to investigate the temperature dependence of the enhancement factor [11]. It is possible to evaluate  $A_{Xe,1}^{iso}$  systematically by first-principles electronic-structure calculations, as discussed below.  $A_{Xe,1}^{iso}$  provides a quantum-chemical equivalent of the enhancement factor.

### D. NMR frequency shift

The  $^{129}\text{Xe}$  NMR frequency shift is induced by the same hyperfine interaction term in the spin Hamiltonian that was used to compute the effective field on the unpaired electron (see above). Hence, we can directly write

$$\Delta\nu_{Xe} = \frac{\Delta E}{h} = \frac{A_{Xe}^{iso} \langle S_z \rangle \Delta m}{h} = \frac{A_{Xe}^{iso}}{h} \langle S_z \rangle \quad (21)$$

TABLE I. Fit parameters for the computational  $^{129}\text{Xe}$  HFCC curve specified by Eq. (26).

Parameter	Value
$B$ (MHz Å)	$-6.0110566354 \times 10^2$
$p_0$	$-1.2851613261 \times 10^0$
$p_1$ (Å $^{-1}$ )	$2.8475138874 \times 10^{-1}$
$p_2$ (Å $^{-2}$ )	$3.4922042825 \times 10^{-2}$

since  $\Delta m = 1$ . By applying the virial expansion for  $^{129}\text{Xe}$  HFCC in the Rb-Xe mixture, we arrive at

$$A_{\text{Xe}}^{\text{iso}} \approx A_{\text{Xe},1}^{\text{iso}}[\text{Rb}], \quad (22)$$

$$\Delta\nu_{\text{Xe}} = \frac{1}{h} A_{\text{Xe},1}^{\text{iso}}[\text{Rb}] \langle S_z \rangle. \quad (23)$$

As before, these expressions are limited to the effects of pairwise interactions in the Rb-Xe dimers present in the gas. To obtain first-principles estimates for the EPR and NMR frequency shifts, we employ quantum-chemical methods to obtain an estimate for  $A_{\text{Xe},1}^{\text{iso}}$  that is as accurate as feasible. This entails the calculation of both the pair interaction potential and  $^{129}\text{Xe}$  HFCC as functions of the Rb-Xe internuclear distance.

### E. Second virial coefficient of $^{129}\text{Xe}$ hyperfine coupling

Observable  $A$  of an isotropic medium can be written as a semiclassical virial expansion [12]

$$\langle A([n], T) \rangle - A_0 = A_1(T)[n] + A_2(T)[n]^2 + \dots, \quad (24)$$

involving dependence on both the number density  $[n]$  of the gas component  $n$  and temperature  $T$ . The terms with increasing power of  $[n]$  in the expansion involve corrections to the average value of  $A$  for a noninteracting molecule  $A_0$  and due to pair, three-body, etc., interactions. In the present problem, the first correction over the vanishing  $^{129}\text{Xe}$  HFCC *in vacuo* arises from the pair interactions between the Xe and Rb atoms (see also Refs. [10,17] for a related formulation):

$$A_{\text{Xe},1}^{\text{iso}}(T) = 4\pi \int_0^\infty A(R) \exp[-V(R)/(kT)] R^2 dR, \quad (25)$$

where  $A(R)$  is the  $^{129}\text{Xe}$  HFCC in the Rb-Xe dimer at the internuclear distance of  $R$ . The calculation involves also the Rb-Xe PEC  $V(R)$ . We use our best theoretical Rb-Xe potential (see Sec. III D) for all the calculations of the second virial coefficient according to Eq. (25). It has been shown that the semiclassical approach employed here is in excellent agreement with a fully quantum mechanical treatment in related noble-gas systems [28] in the experimental temperature range relevant for SEOP processes. The temperature dependence of our results is tabulated in Table I in the Supplemental Material [29] in the temperature range of 50–500 K.

## III. COMPUTATIONS

### A. Hyperfine coupling

Nonrelativistic (NR) all-electron density-functional theory (DFT) calculations of  $A(R)$  were performed with the ORCA

[30] software package, using the Perdew-Burke-Ernzerhof (PBE) exchange-correlation functional [31], its one-parameter hybrid variant (PBE0) [32–34], the Becke-Lee-Yang-Parr (BLYP) functional consisting of Becke 1988 exchange [35] and Lee-Yang-Parr correlation [36,37] parts, and the Becke three-parameter Lee-Yang-Parr (B3LYP) hybrid functional [36,38–40]. Additionally, correlated *ab initio* calculations at the second-order Møller-Plesset perturbation (MP2) and coupled-cluster single, double, and perturbative triple excitations [CCSD(T)] levels of theory were performed with the CFOUR [41] program. Furthermore, fully relativistic (R) four-component (with noncollinear magnetization) calculations of the HFCC were carried out in the matrix Dirac-Kohn-Sham framework [42] using a restricted, kinetically balanced basis set (mDKS-RKB) [43] in the RESPECT software [44] by using the same DFT functionals as mentioned above.

For the development of the basis set, we used a local version of the KRUUNUNHAKA basis-set toolkit that employs the completeness-optimization method [45], like in our earlier publications [46–50]. The same final, uncontracted basis was used for both Rb and Xe atoms as the completeness-optimized basis sets are element independent. The basis consists of  $27s25p21d1f$  primitives and contains 428 basis functions for the Rb-Xe dimer. This basis was also used for the large-component wave function in the mDKS-RKB calculations. The exponents of this basis set are listed in Table I of the Supplemental Material of Ref. [50]. Using the final basis, the basis-set error of the HFCCs was monitored to be maximally about 1% at the NR B3LYP level (representing DFT in general here) at Rb-Xe internuclear distances of 3.6 and 4.6 Å. A larger basis set was used to assess the basis-set deficiency at the correlated *ab initio* MP2 level of theory. This basis was augmented with three additional  $f$  functions per atom compared to the original basis and contained a total of 470 basis functions. The exponents of  $f$  functions are listed in Table S2 of the Supplemental Material of Ref. [51]. We tested the larger basis set at three Rb-Xe internuclear distances, 3, 5.4, and 7 Å, to provide an estimate of the basis-set error, by which we corrected the CCSD(T) results obtained with the 428-function basis. The results thus corrected are denoted “bascorr” in the following. The relative magnitude of the correction turned out to be less than 2% of the HFCC in all cases.

A subset of the HFCCs and their differences are plotted as a function of the Rb-Xe internuclear distance in Fig. 1. Our current best results, obtained in the piecewise approximated fashion at the R PBE0+NR CCSD(T)(bascorr)–NR PBE0 level of theory (see below), are presented in Fig. 1(a). Relativity plays a major role, as observed from the difference of the PBE0 results in the NR and R regimes. In particular, this difference is very pronounced at small internuclear distances. The basis-set correction (bascorr) performed on top of the CCSD(T) data at the MP2 level of theory shows up as only a small negative shift of the HFCC throughout the distance range. At long internuclear distances, all the Xe HFCCs in the Rb-Xe system behave very similarly due to the fact that the HFCC of the closed-shell Xe atom must decay to zero when the Rb atom and its unpaired electron are far away.

In Fig. 1(b), the differences between our best calculated values and those calculated at lower levels of approximation are presented. We note that all the NR computational methods

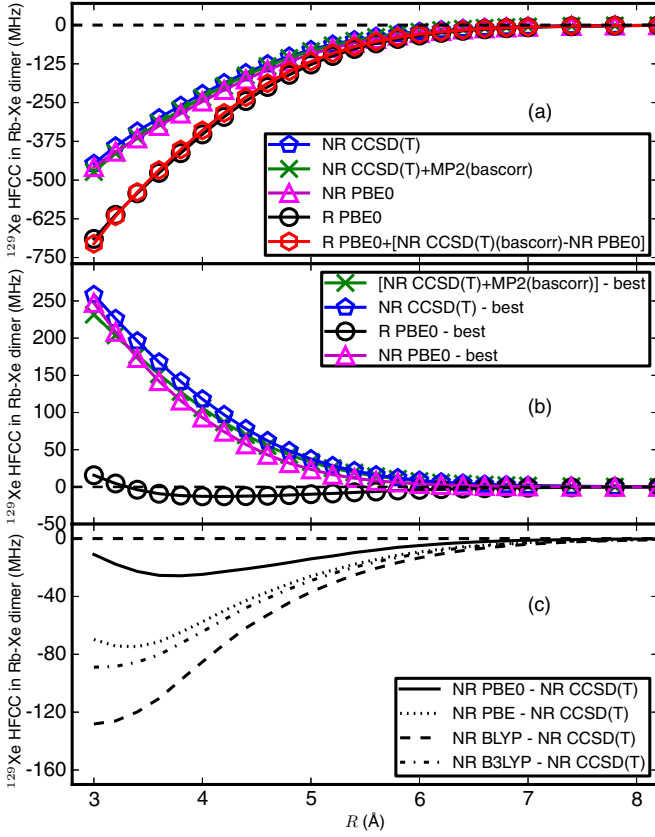


FIG. 1. Calculated  $^{129}\text{Xe}$  hyperfine coupling constant (HFCC) in the Rb-Xe dimer as a function of the Rb-Xe internuclear distance. (a) Results with our best current level of theory with a piecewise approximate treatment, relativistic PBE0 + [nonrelativistic CCSD(T)(bascorr)–nonrelativistic PBE0], as well as several other lower-level approximations. (b) The calculated difference curves between our best and lower-level HFCC values. (c) The calculated difference curves between our best nonrelativistic HFCC values and curves calculated with various lower-level nonrelativistic methods.

produce a distinct increase in the magnitude of the HFCC values and that the R PBE0 values are very close to our best curve. In Fig. 1(c), our preferred choice of the exchange-correlation functional (PBE0) is justified in the NR regime. Here, the calculated differences between NR CCSD(T) and the results of various exchange-correlation functionals are presented. We observe that the difference between the NR CCSD(T) and NR PBE0 results for the  $^{129}\text{Xe}$  HFCC in the Rb-Xe system is very small, thereby motivating the choice of the relativistic PBE0 as a starting point for our piecewise additive scheme presented in Eq. (26) below.

### B. Fitting of the hyperfine coupling constants

To employ the HFCCs and PECs in the calculation of  $A_{\text{Xe},1}^{\text{iso}}$  according to Eq. (25), both quantities were fitted to functional forms. To fit the HFCC, we used the following piecewise additive scheme [52]:

$$A = \text{R PBE0} + [\text{NR CCSD(T)(bascorr)} - \text{NR PBE0}], \quad (26)$$

where R and NR denote fully relativistic and nonrelativistic calculations and the term bascorr refers to the basis-set

correction carried out at the MP2 level of theory as

$$\begin{aligned} \text{NR CCSD(T)(bascorr)} = & \text{NR CCSD(T)(final basis)} \\ & + [\text{NR MP2(larger basis)} \\ & - \text{NR MP2(final basis)}]. \quad (27) \end{aligned}$$

The basis sets employed are explained in Sec. III A. The first term in Eq. (26) includes the combined effect of relativity and correlation at the selected DFT level of theory, whereas the second part evaluates more accurately the effect of electron correlation in the NR regime. DFT with the PBE0 functional was employed, accompanied by high-level *ab initio* calculations of HFCC at the CCSD(T) level of theory [53]. Such a piecewise scheme is resorted to because, currently, we do not have a rigorous means to compute the HFCC at the fully relativistic, electron-correlated *ab initio* level of theory. Hence, this scheme is an approximation.

To reproduce the internuclear distance dependence of the best piecewise approximated HFCC data as accurately as possible, we used our standard fitting function [20,52,54]:

$$A(R) = C/R^{p(R)}, \quad (28)$$

$$p(R) = p_0 + p_1 R + p_2 R^2, \quad (29)$$

where  $C$  and  $p_0$ – $p_2$  are adjustable parameters. Furthermore, we used an additional weight function

$$W(R) = \exp[-V(R)/(kT)], \quad (30)$$

which employs our current best PEC,  $V(R)$ , on the residual error between the fit function and the quantum-mechanical HFCC data points, with the temperature parameter  $T = 1300$  K. This was done to emphasize the role of the thermally accessible range of the Rb-Xe internuclear distances in the fit parameters. A high value of the temperature parameter serves to enhance the probing of the small  $R$  values at which the largest  $^{129}\text{Xe}$  HFCCs occur. The fit parameters for our best data according to Eq. (26) are given in Table I.

### C. Rb-Xe potential-energy curve

The PECs for the Rb-Xe dimer were calculated at correlated, unrestricted MP2, CCSD, and CCSD(T) levels of theory with the MOLPRO [55] program package. Motivated by, e.g., our earlier work with the Xe-Xe interaction potential [20], large valence basis sets with the inclusion of bond basis functions [56], as well as relativistic effective core potentials (ECPs), were used. We calculated the best current PEC at the CCSD(T) level using a relativistic ECP (RECP28MDF) for both Rb [57] and Xe [58], together with the valence basis sets of augmented correlation-consistent polarized valence pentuple-zeta (aug-cc-pV5Z) quality for Rb [57] and Xe [58]. These basis sets were manually supplemented with three (two) sets of primitive diffuse *spdfgh* functions for Rb (Xe), with Gaussian exponents selected using the rule of thumb  $\zeta_i/\zeta_{i-1} = \frac{1}{3}$  (starting from the lowest exponent already present). Furthermore, a specific  $3s3p2d2f1g$  set of bond basis functions with standard exponents taken from Refs. [56,59,60] was added. In particular, the last diffuse  $h$  exponent for the atomic basis set of Rb was taken from the Kr valence basis set corresponding to the relativistic ECP10MDF

TABLE II. Experimental and calculated enhancement factor  $\kappa$  for the Rb-Xe spin-exchange optical pumping process at different temperatures.

Experimental			Calculated		
$T$ (°C)	$\kappa$	Ref.	$T$ (°C)	$\kappa$	Ref.
80	$640 \pm 350$	[10]	100	$720 \pm 290$	[10]
140–220	$493 \pm 31$	[11]	142–227	$588 \pm 50$	Current work
150	$520 \pm 20$	[25]			

pseudopotential [58]. The lowest  $h$  exponent was then obtained with the above “ $\frac{1}{3}$  rule.” The final atomic basis set has the structure  $(38s32p26d14f10g7h)/[24s23p18d14f10g7h]$  for the Rb-Xe system, using the (primitive)/(contracted) notation. The exponents (except for the midbond basis functions [56]) are listed in Table II in the Supplemental Material [29]. The total number of basis functions (including the midbond basis functions) was 529 for the Rb-Xe dimer. The basis-set superposition error (BSSE) was corrected for using the counterpoise method [61]. Close to the equilibrium distance, at 5.4 Å, this correction amounts to no less than 157 K for the Rb-Xe potential well, which has a depth of 146 K after the correction. This underlines the need for taking care of BSSE within very shallow potential wells.

The effect of various electron-correlation treatments at the MP2, CCSD, and CCSD(T) levels on the Rb-Xe PEC is illustrated in Fig. 2. The unrestricted Hartree-Fock (UHF) theory fails to produce any potential well. The usual overestimation of the well depth is observed with the MP2 theory. CCSD reduces the well depth drastically, and the currently best results, obtained at the CCSD(T) level, are located between CCSD and MP2, relatively close to the latter.

#### D. Fitting of the interaction potentials

To fit the PEC, an Aziz-Slaman-type interaction potential, the so-called Hartree-Fock dispersion B form [62] was used,

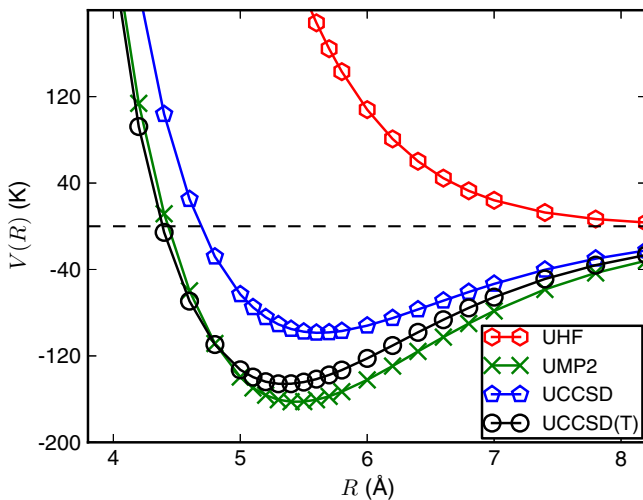


FIG. 2. BSSE-corrected Rb-Xe potential-energy curves at the unrestricted (U) Hartree-Fock (HF) and various post-HF [UMP2, UCCSD, and UCCSD(T)] levels of theory with the final basis set (see text).

the details of which can be found in the Supplemental Material [29]. The fitting parameters of our best Rb-Xe PEC are given in the Supplemental Material [29]. The obtained potential well depth,  $D_e = 142.26$  K, of our best theoretical Rb-Xe PEC agrees to some extent with the literature value of  $D_e$  of 125.36 K by Patil [63], who used a combination of theoretical calculations and empirical values for some of the parameters, and very well with the value of 143.36 K from Refs. [64,65], which employed first-principles calculations. For the equilibrium distance  $R_e$ , the values of 5.4082 Å [63,64] and 5.4248 Å [65] have been obtained, which should be contrasted with our present result,  $R_e = 5.3674$  Å. In conclusion, as a secondary result of this study, probably one of the best theoretical PECs for the Rb-Xe system has been produced.

## IV. ELECTRONIC AND NUCLEAR POLARIZATION

### A. Hyperfine coupling

The EPR and  $^{129}\text{Xe}$  NMR frequency shifts (in Hz) can thus be obtained from Eqs. (19) and (23), respectively. We have determined the electron spin polarization ( $S_z$ ) appearing in the latter equation by assuming that Killian’s relation [21] between the temperature and the Rb number density [Rb] is valid for the relevant experimental conditions. Killian developed an empirical relation between the pressure and temperature of Rb vapor by measuring the positive-ion emission as a function of filament temperature [21]. Hence, [Rb] in Killian’s relation depends on only the temperature of the measurement.  $A_{\text{Xe},1}^{\text{iso}}(T)$  contains the effect of the hyperfine coupling between the Xe nucleus and the unpaired electron of Rb, averaged over the Rb-Xe PEC. Note that we do not use the empirical enhancement factor  $\kappa$  in these formulas, but rather describe the frequency shifts in terms of the microscopic molecular property,  $^{129}\text{Xe}$  HFCC. We use the leading term in the virial expansion [12] for the evaluation of this quantity in the gas mixture of Rb and Xe, in close analogy to the case of chemical shift in dilute monoatomic Xe gas [20,52]. Furthermore,  $A_{\text{Xe},1}^{\text{iso}}$  holds an inherent temperature dependence, which allows for a direct comparison with the experimental temperature dependence of  $\kappa$  as well. The enhancement factor can be conveniently written in terms of  $A_{\text{Xe},1}^{\text{iso}}$  [Eq. (20)], as discussed in Sec. II C. Our formulation includes naturally the contributions to the enhancement factor by both instantaneous binary collisions and persistent van der Waals dimers [10,11].  $A_{\text{Xe},1}^{\text{iso}}$  does not contain a reference to the duration of the interaction between Xe and Rb. Instead, it probes both regimes due to the thermally averaged internuclear Rb-Xe distance-dependent  $^{129}\text{Xe}$  HFCC.

Quantum-mechanical methodology was used to compute  $A_{\text{Xe},1}^{\text{iso}}$ , as described in Sec. II. In Fig. 3, the calculated temperature dependence of  $A_{\text{Xe},1}^{\text{iso}}$  is plotted at various levels of theory. As the same Rb-Xe PEC was used for all the calculations of  $A_{\text{Xe},1}^{\text{iso}}$ , these curves directly reflect the properties of the HFCC obtained using different computational approximations. A distinct difference between the NR and relativistic DFT results, obtained with the PBE0 [31–34] functional, is observed throughout the temperature range. On top of that, the effects of electron correlation are calculated as

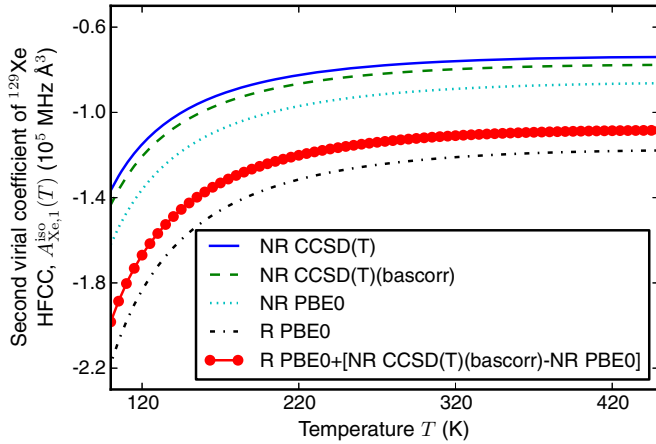


FIG. 3. Calculated temperature dependence of the second virial coefficient of the  $^{129}\text{Xe}$  hyperfine coupling constant (HFCC)  $A_{\text{Xe},1}^{\text{iso}}(T)$  using the best current theoretical Rb-Xe potential-energy curve, as well as several different approximations for the  $^{129}\text{Xe}$  HFCC in the Rb-Xe dimer. For notation, see Sec. III B.

the difference between the *ab initio* CCSD(T) level of theory and NR PBE0, providing only a small positive shift. Our best piecewise approximated results are denoted as R PBE0 + [NR CCSD(T)(bascorr)–NR PBE0], where bascorr refers to the basis-set correction performed at the MP2 theory level, as described above. Contrary to the results for  $\kappa$  in the Rb- $^3\text{He}$  mixture [13], the temperature dependence of the present equivalent parameter  $A_{\text{Xe},1}^{\text{iso}}$  is very weak in the experimentally relevant temperature range. This is not surprising since the Rb-He PEC is much shallower and less steep than its Rb-Xe counterpart.

### B. Electronic spin

In Fig. 4, we plot the degree of electron spin polarization  $P_S$  as a function of the  $^{129}\text{Xe}$  NMR frequency shift, based on Eq. (23), the calculated  $A_{\text{Xe},1}^{\text{iso}}$ , and assuming that Killian’s formula [21] for the Rb number density [Rb] holds at these temperatures. The Rb electron spin polarization is calculated at the experimentally observed Xe NMR frequency shifts estimated from the positions of peak maxima in Fig. 1 of Ref. [11], as well as taken directly from Table 2.2 of Ref. [66].

We obtain an electron spin polarization of the order of 80% (see Fig. 4). Different estimates for the polarization, dependent on the experimental conditions such as laser power, temperature, and xenon number density, exist in the literature, ranging from 10%–80% [67] to 10%–60% [68]. The former values are based on numerical simulations, and the latter are measured ones. In particular, Liu *et al.* [69] have estimated the polarization to be in the range of 60%–70% in a Rb-Xe SEOP experiment, based on the measured experimental frequency shifts and the  $\kappa$  value of  $493 \pm 31$  [11].

### C. Nuclear spin

In Fig. 5 we show the degree of xenon nuclear spin polarization as a function of the EPR frequency shift at different values of temperature and the Xe number density [Xe]. The data are based on Eq. (19). In this plot we have

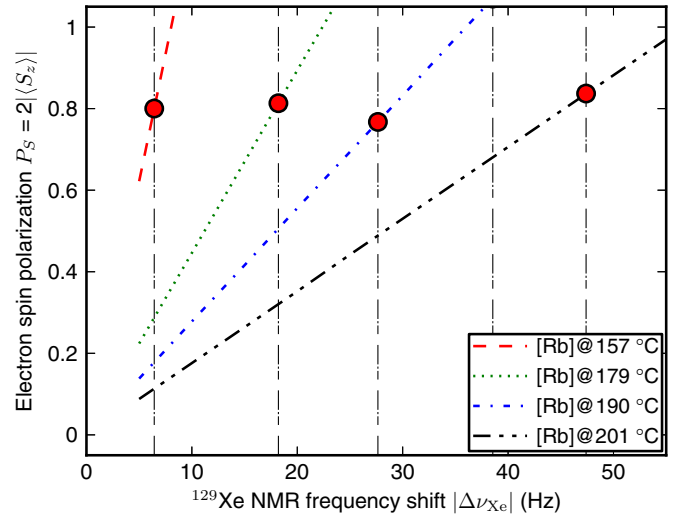


FIG. 4. Calculated degree of electron spin polarization at different temperatures and Rb number densities in a Rb-Xe gas admixture, computed from Eq. (23) as a function of the  $^{129}\text{Xe}$  NMR frequency shift. The [Rb] number density is estimated based on the relation by Killian [21]. The vertical dashed lines correspond to the experimentally measured frequency shifts [11,66] at temperatures of 157 °C, 179 °C, 190 °C, 190 °C, and 201 °C (from left to right). The red spheres depict intersections between vertical and [Rb] lines at the corresponding temperatures. Note that the fourth vertical line corresponding to the temperature of 190 °C does not intersect with the [Rb]@190 °C line at a physically meaningful ( $P_S \leq 1$ ) value.

a handful of observed EPR frequency shifts that have been employed to predict  $P_{\text{Xe}}$  at different [Xe]. We observe that the temperature has only a small effect on  $P_{\text{Xe}}$  due to the small inherent temperature dependence of the calculated  $A_{\text{Xe},1}^{\text{iso}}$ , as mentioned above. A similar observation was experimentally made for the related quantity  $\kappa$  [10,11], now verified in terms of first-principles calculations. In contrast, the effect of [Xe] on  $P_{\text{Xe}}$  is much larger than that of the temperature. The experimental conditions ( $T$ , [Xe]) for which the results of Fig. 5 have been computed are due to the works of Ma, Sorte, and Saam [11,66] and Bear [70], as well as on-going measurements [25]. The two distinctly marked data points represent the calculated values of  $P_{\text{Xe}}$  at the observed EPR frequency of 2.76 kHz, which is due to the work of Bear, using the computed enhancement factor  $\kappa$  of 726 from Schaefer *et al.* [10], and the present calculations using our result,  $\kappa = 588$  (see below). There is a difference between our  $P_{\text{Xe}}$  values of roughly 10%–40% and the ones measured in the experiments,  $P_{\text{Xe}} \approx 60\%$ –70% [1,71,72]. However, as noted already in the context of electron spin polarization, several factors, such as the partial pressure of xenon, xenon and rubidium number densities, laser power, wall relaxation, etc., all play a role in the experimental setups referred to in Fig. 5 [11,66,70], as well as in more recent studies [1,71,72].

### D. Enhancement factor

Table II presents the available results for  $\kappa$  from both experimental and theoretical work reported in the literature. Our own datum,  $\kappa = 588$ , is based on the calculated  $A_{\text{Xe},1}^{\text{iso}}$

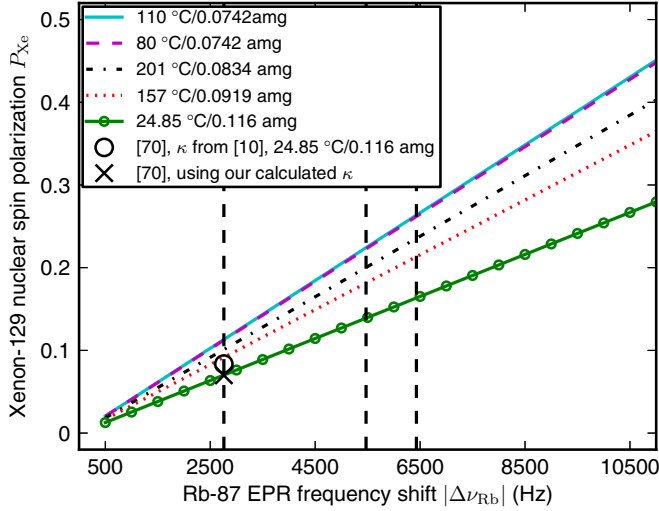


FIG. 5. Calculated degree of absolute  $^{129}\text{Xe}$  nuclear spin polarization  $P_{\text{Xe}}$  computed from Eq. (19) as a function of the  $^{87}\text{Rb}$  EPR frequency shift for the same combinations of experimental temperature and Xe number density (expressed in amagat units, amg). The three observed EPR frequencies of 2.76, 5.47, and 6.43 kHz [11,25,66,70] are highlighted as vertical dashed lines in the plot. The effect of temperature on  $P_{\text{Xe}}$  is very small, as observed in the nearly overlapping lines labeled 110 °C and 80 °C at  $[\text{Xe}]$  of 0.0742 amagat.

[Eq. (20)] in the temperature range of 142 °C–227 °C. To estimate the error of our  $\kappa$ , we replaced the CCSD(T) by MP2 results, which yielded an absolute change of roughly 2 units in the computed  $\kappa$ . The difference of these two PECs serves as a conservative estimate of the systematic error due to  $V(R)$ , which is found to be quite small. In a similar vein, changing the PBE0 functional to B3LYP in the HFCC curve produces an absolute change of 30 units in the computed  $\kappa$  parameter. Furthermore, the remaining basis-set errors in the HFCC are estimated (with MP2; see Sec. III A) to amount to less than 20 units in the final calculated  $\kappa$  (see below). The combined error from all these sources is estimated at 50 units. Thus, we can state that our result,  $\kappa = 588 \pm 50$ , agrees moderately well with the most recent published experiment stating  $\kappa = 493 \pm 31$  [11] and constitutes a major improvement over the previous theoretical estimate of  $720 \pm 290$  [10]. Preliminary results of the most recent measurements of  $\kappa = 520 \pm 20$  (150 °C) [25] point to the conclusion that the current purely theoretical estimate is, in fact, in excellent agreement with experiment.

Accurate calculations of  $A_{\text{Xe},1}^{\text{iso}}$  provide a tool for accessing the important and experimentally nontrivial parameters  $P_{\text{Xe}}$  and  $P_S$  within SEOP processes. Based on Eqs. (19)–(23), these parameters can be written as

$$P_{\text{Xe}} = 2\langle I_z \rangle \approx 3.05 \times \frac{\Delta\nu_{\text{Rb}}(\text{Hz})}{a[\text{Xe}]} 10^{-6}, \quad (31)$$

$$P_S = 2\langle S_z \rangle \approx 6.86 \times \frac{\Delta\nu_{\text{Xe}}(\text{Hz})}{[\text{Rb}]} 10^{-7} \quad (32)$$

at a temperature of 157 °C. Here, the average value of  $-108\,500 \text{ MHz } \text{\AA}^3$  was used for  $A_{\text{Xe},1}^{\text{iso}}$ , calculated at our

preferred R PBE0 + [NR CCSD(T)(bascorr)–NR PBE0] level of theory. Both  $[\text{Xe}]$  and  $[\text{Rb}]$  are given in amagat units in Eqs. (31) and (32). Furthermore, we assume in Eq. (31) that enriched xenon gas with an abundance factor of  $a$  for the  $^{129}\text{Xe}$  isotope ( $a = 0-1$ ) is used. We note that the temperature dependence of  $P_{\text{Xe}}$  is modest, which follows from the nearly flat temperature behavior of  $A_{\text{Xe},1}^{\text{iso}}$  at the experimentally relevant temperature range (see Fig. 3). The estimated error of 50 units (10%) in  $A_{\text{Xe},1}^{\text{iso}}$  transfers readily to the spin polarizations as well since both of these quantities are directly calculated from Eqs. (19)–(23). It should be noted that this error is a result of a rather conservative estimation.

## V. CONCLUSIONS

We presented a first-principles-assisted evaluation of the experimentally crucial physical parameters in SEOP experiments, the degrees of Rb electron spin and  $^{129}\text{Xe}$  nuclear spin polarization in the relevant experimental conditions, a dilute Rb-Xe gas mixture. To access these parameters, we used the experimentally measured NMR and EPR frequency shifts in combination with high-level electronic-structure calculations of the  $^{129}\text{Xe}$  hyperfine coupling constant in the Rb-Xe dimer averaged over the state-of-the-art Rb-Xe interaction potential, as well as a well-known empirical relation between temperature and the Rb number density. A pairwise approximation in the form of the leading interaction term in the virial expansion of the  $^{129}\text{Xe}$  HFCC was employed. We provided a purely theoretical, temperature-dependent estimate of the well-known SEOP enhancement factor  $\kappa$  via first-principles all-electron calculations of the second virial coefficient of  $^{129}\text{Xe}$  HFCC in the Rb-Xe gas mixture. The result equals 588 in the experimentally relevant temperature range, in line with the preliminary most recent experimental measurement,  $\kappa \approx 520$  (at 150 °C). The present results should be useful for assessing the physical conditions of SEOP experiments and may aid in the design and construction of new types of HP equipment in the future.

## ACKNOWLEDGMENTS

M.H. acknowledges funding from the Finnish Society of Sciences and Letters. P.L. is supported by the Academy of Finland, Project No. 285666. M.R. acknowledges support from the Research Council of Norway (RCN) through a Center of Excellence (CoE) Grant (Grant No. 179568) and the computational resources provided by the NOTUR high-performance computing program (Grant No. NN4654K). J.M. and J.V. have obtained support from the Academy of Finland (Projects No. 258565 and No. 296292), as well as from the People Programme (Marie Curie Actions) of the European Union's Seventh Framework Programme FP7/2007-2013 under REA Grant Agreement No. 317127. The computational resources were partially provided by CSC IT Center for Science (Espoo, Finland) and the Finnish Grid Infrastructure (FGI) project.

- [1] P. Nikolaou, A. M. Coffey, L. L. Walkup, B. M. Gust, N. Whiting, H. Newton, S. Barcus, I. Muradyan, M. Dabaghyan, G. D. Moroz, M. S. Rosen, S. Patz, M. J. Barlow, E. Y. Chekmenev, and B. M. Goodson, *Proc. Natl. Acad. Sci. USA* **110**, 14150 (2013).
- [2] P. Nikolaou, A. M. Coffey, L. L. Walkup, B. M. Gust, C. D. LaPierre, E. Koehnemann, M. J. Barlow, M. S. Rosen, B. M. Goodson, and E. Y. Chekmenev, *J. Am. Chem. Soc.* **136**, 1636 (2014).
- [3] M. Kirby, S. Svenningsen, A. Owrangi, A. Wheatley, A. Farag, A. Ouriadov, G. E. Santyr, R. Etemad-Rezai, H. O. Coxson, D. G. McCormack, and G. Parraga, *Radiology* **265**, 600 (2012).
- [4] D. M. Lilburn, A. L. Tatler, J. S. Six, C. Lesbats, A. Habgood, J. Porte, T. Hughes-Riley, D. E. Shaw, G. Jenkins, and T. Meersmann, *Magn. Reson. Med.* **76**, 1224 (2016).
- [5] I. M. Savukov and M. V. Romalis, *Phys. Rev. Lett.* **94**, 123001 (2005).
- [6] L. Schröder, *Phys. Med.* **29**, 3 (2013).
- [7] M. G. Shapiro, R. M. Ramirez, L. J. Sperling, G. Sun, J. Sun, A. Pines, D. V. Schaffer, and V. S. Bajaj, *Nat. Chem.* **6**, 629 (2014).
- [8] R. Jiménez-Martínez, D. J. Kennedy, M. Rosenbluh, E. A. Donley, S. Knappe, S. J. Seltzer, H. L. Ring, V. S. Bajaj, and J. Kitching, *Nat. Commun.* **5**, 3908 (2014).
- [9] T. G. Walker and W. Happer, *Rev. Mod. Phys.* **69**, 629 (1997).
- [10] S. R. Schaefer, G. D. Cates, T.-R. Chien, D. Gonatas, W. Happer, and T. G. Walker, *Phys. Rev. A* **39**, 5613 (1989).
- [11] Z. L. Ma, E. G. Sorte, and B. Saam, *Phys. Rev. Lett.* **106**, 193005 (2011).
- [12] A. D. Buckingham and J. A. Pople, *Discuss. Faraday Soc.* **22**, 17 (1956).
- [13] M. V. Romalis and G. D. Cates, *Phys. Rev. A* **58**, 3004 (1998).
- [14] T. V. Tscherbul, P. Zhang, H. R. Sadeghpour, A. Dalgarno, N. Brahms, Y. S. Au, and J. M. Doyle, *Phys. Rev. A* **78**, 060703 (2008).
- [15] T. V. Tscherbul, P. Zhang, H. R. Sadeghpour, and A. Dalgarno, *Phys. Rev. A* **79**, 062707 (2009).
- [16] T. V. Tscherbul, P. Zhang, H. R. Sadeghpour, and A. Dalgarno, *Phys. Rev. Lett.* **107**, 023204 (2011).
- [17] T. G. Walker, *Phys. Rev. A* **40**, 4959 (1989).
- [18] N. Brahms, T. V. Tscherbul, P. Zhang, J. Kłos, H. R. Sadeghpour, A. Dalgarno, J. M. Doyle, and T. G. Walker, *Phys. Rev. Lett.* **105**, 033001 (2010).
- [19] N. Tariq, N. A. Taisan, V. Singh, and J. D. Weinstein, *Phys. Rev. Lett.* **110**, 153201 (2013).
- [20] M. Hanni, P. Lantto, N. Runeberg, J. Jokisaari, and J. Vaara, *J. Chem. Phys.* **121**, 5908 (2004).
- [21] T. J. Killian, *Phys. Rev.* **27**, 578 (1926).
- [22] M. Siefert, A. Liebisch, B. Blümich, and S. Appelt, *Nat. Phys.* **11**, 767 (2015).
- [23] G. Breit and I. I. Rabi, *Phys. Rev.* **38**, 2082 (1931).
- [24] The minus sign corresponds to  $F = I - S$ .
- [25] B. Saam (unpublished).
- [26] J. Fukutomi, E. Suzuki, T. Shimizu, A. Kimura, and H. Fujiwara, *J. Magn. Reson.* **160**, 26 (2003).
- [27] S. Bize, Y. Sortais, M. S. Santos, C. Mandache, A. Clairon, and C. Salomon, *Europhys. Lett.* **45**, 558 (1999).
- [28] A. Antušek, M. Jaszuński, and A. Rizzo, *J. Chem. Phys.* **126**, 074303 (2007).
- [29] See Supplemental Material at <http://link.aps.org/supplemental/10.1103/PhysRevA.95.032509> for the temperature dependence of the second virial coefficient of Xe hyperfine coupling, for the basis set used to obtain the Rb-Xe PEC, and for the fitting details of the calculated potential-energy curves.
- [30] F. Neese, ORCA, an *ab initio*, density functional and semiempirical program package, version 2.9, Max Planck Institute of Bioinorganic Chemistry, Munich, 2012.
- [31] J. P. Perdew, K. Burke, and M. Ernzerhof, *Phys. Rev. Lett.* **77**, 3865 (1996); **78**, 1396(E) (1997).
- [32] J. P. Perdew, M. Ernzerhof, and K. Burke, *J. Chem. Phys.* **105**, 9982 (1996).
- [33] C. Adamo and V. Barone, *Chem. Phys. Lett.* **298**, 113 (1998).
- [34] C. Adamo and V. Barone, *J. Chem. Phys.* **110**, 6158 (1999).
- [35] A. D. Becke, *Phys. Rev. A* **38**, 3098 (1988).
- [36] C. Lee, W. Yang, and R. G. Parr, *Phys. Rev. B* **37**, 785 (1988).
- [37] B. Miehlich, A. Savin, H. Stoll, and H. Preuss, *Chem. Phys. Lett.* **157**, 200 (1989).
- [38] S. H. Vosko, L. Wilk, and M. Nusair, *Can. J. Phys.* **58**, 1200 (1980).
- [39] A. D. Becke, *J. Chem. Phys.* **98**, 5648 (1993).
- [40] P. J. Stephens, F. J. Devlin, C. F. Chabalowski, and M. J. Frisch, *J. Phys. Chem.* **98**, 11623 (1994).
- [41] CFOUR, a quantum-chemical program package written by J. F. Stanton, J. Gauss, M. E. Harding, and P. G. Szalay with contributions from A. A. Auer, R. J. Bartlett, U. Benedikt, C. Berger, D. E. Bernholdt, Y. J. Bomble, L. Cheng, O. Christiansen, M. Heckert, O. Heun, C. Huber, T.-C. Jagau, D. Jonsson, J. Jusélius, K. Klein, W. J. Lauderdale, D. A. Matthews, T. Metzroth, L. A. Mück, D. P. O'Neill, D. R. Price, E. Prochnow, C. Puzzarini, K. Ruud, F. Schiffmann, W. Schwalbach, C. Simmons, S. Stopkowicz, A. Tajti, J. Vázquez, F. Wang, and J. D. Watts and the integral packages MOLECULE (J. Almlöf and P. R. Taylor), PROPS (P. R. Taylor), and ABACUS (T. Helgaker, H. J. Aa. Jensen, P. Jørgensen, and J. Olsen) and ECP routines by A. V. Mitin and C. van Wüllen. For the current version, see <http://www.cfour.de>.
- [42] E. Malkin, M. Repiský, S. Komorovský, P. Mach, O. L. Malkina, and V. G. Malkin, *J. Chem. Phys.* **134**, 044111 (2011).
- [43] M. Repiský, S. Komorovský, E. Malkin, O. L. Malkina, and V. G. Malkin, *Chem. Phys. Lett.* **488**, 94 (2010).
- [44] M. Repiský, S. Komorovský, V. G. Malkin, O. L. Malkina, M. Kaupp, and K. Ruud, with contributions from R. Bast, U. Ekström, S. Knecht, I. Malkin Ondik, and E. Malkin, RESPECT, relativistic spectroscopy DFT program, version 3.3.0, <http://www.respectprogram.org>.
- [45] P. Manninen and J. Vaara, *J. Comput. Chem.* **27**, 434 (2006).
- [46] S. Ikäläinen, P. Lantto, P. Manninen, and J. Vaara, *J. Chem. Phys.* **129**, 124102 (2008).
- [47] S. Ikäläinen, P. Lantto, P. Manninen, and J. Vaara, *Phys. Chem. Chem. Phys.* **11**, 11404 (2009).
- [48] S. Ikäläinen, M. V. Romalis, P. Lantto, and J. Vaara, *Phys. Rev. Lett.* **105**, 153001 (2010).
- [49] J. Jokisaari and J. Vaara, *Phys. Chem. Chem. Phys.* **15**, 11427 (2013).
- [50] J. Vaara, M. Hanni, and J. Jokisaari, *J. Chem. Phys.* **138**, 104313 (2013).
- [51] J. Roukala, J. Zhu, C. Giri, K. Rissanen, P. Lantto, and V.-V. Telkki, *J. Am. Chem. Soc.* **137**, 2464 (2015).
- [52] M. Hanni, P. Lantto, M. Iliaš, H. J. Aa. Jensen, and J. Vaara, *J. Chem. Phys.* **127**, 164313 (2007).

- [53] J. D. Watts, J. Gauss, and R. J. Bartlett, *Chem. Phys. Lett.* **200**, 1 (1992).
- [54] J. Kantola, J. Vaara, T. T. Rantala, and J. Jokisaari, *J. Chem. Phys.* **107**, 6470 (1997).
- [55] H.-J. Werner, P. J. Knowles, G. Knizia, F. R. Manby, and M. Schütz, *WIREs Comput. Mol. Sci.* **2**, 242 (2012).
- [56] P. Slavíček, R. Kalus, P. Paška, I. Odvárková, P. Hobza, and A. Malijevský, *J. Chem. Phys.* **119**, 2102 (2003).
- [57] I. S. Lim, P. Schwerdtfeger, B. Metz, and H. Stoll, *J. Chem. Phys.* **122**, 104103 (2005).
- [58] K. A. Peterson, D. Figgen, E. Goll, H. Stoll, and M. Dolg, *J. Chem. Phys.* **119**, 11113 (2003).
- [59] F. Tao and Y. Pan, *J. Chem. Phys.* **97**, 4989 (1992).
- [60] F. Tao and Y. Pan, *Chem. Phys. Lett.* **194**, 162 (1992).
- [61] S. F. Boys and F. Bernardi, *Mol. Phys.* **19**, 553 (1970).
- [62] R. A. Aziz and M. J. Slaman, *Mol. Phys.* **57**, 825 (1986).
- [63] S. H. Patil, *J. Chem. Phys.* **94**, 8089 (1991).
- [64] D. Cvetko, A. Lausi, A. Morgante, F. Tommasini, P. Cortona, and M. G. Dondi, *J. Chem. Phys.* **100**, 2052 (1994).
- [65] R.-H. Xie and J. Gong, *Phys. Rev. Lett.* **95**, 263202 (2005).
- [66] Z. Ma, Ph.D. thesis, University of Utah, 2013.
- [67] Z. G. Wang, Q. Y. Jiang, X. Zhan, Y. D. Chen, and H. Luo, *AIP Adv.* **6**, 085110 (2016).
- [68] Z. Ding, X. Long, J. Yuan, Z. Fan, and H. Luo, *Sci. Rep.* **6**, 32605 (2016).
- [69] X. H. Liu, H. Luo, T. L. Qu, K. Y. Yang, and Z. C. Ding, *AIP Adv.* **5**, 107119 (2015).
- [70] D. C. Bear, Ph.D. thesis, Harvard University, 2000.
- [71] D. A. Barskiy, A. M. Coffey, P. Nikolaou, D. M. Mikhaylov, B. M. Goodson, R. T. Branca, G. J. Lu, M. G. Shapiro, V.-V. Telkki, V. V. Zhivonitko, I. V. Koptug, O. G. Salnikov, K. V. Kovtunov, V. I. Bukhtiyarov, M. S. Rosen, M. J. Barlow, S. Safavi, I. P. Hall, L. Schröder, and E. Y. Chekmenev, *Chem. Eur. J.* **23**, 725 (2017).
- [72] N. J. Rogers, F. Hill-Casey, K. F. Stupic, J. S. Six, C. Lesbats, S. P. Rigby, J. Fraissard, G. E. Pavlovskaya, and T. Meersmann, *Proc. Natl. Acad. Sci. USA* **113**, 3164 (2016).